Acta Astronautica 216 (2024) 129–142

Contents lists available at ScienceDirect

Acta Astronautica

journal homepage: www.elsevier.com/locate/actaastro

Research paper

# Feasibility study of a Solar Electric Propulsion mission to Mars

Marco Casanova-Álvarez [a,b,e,*], Fermín Navarro-Medina [a,c], Daniele Tommasini [d,e]

[a] Aerospace Engineering Area, School of Aeronautic and Space Engineering, Universidade de Vigo, As Lagoas s/n, Ourense, 32004, Spain
[b] Earth Explorers Operations Section, European Space Operations Centre, Robert Bosch Str 5, Darmstadt, 64293, Germany
[c] AtlanTTic, Aerospace Technology Research Group, Universidade de Vigo, Vigo, 36310, Spain
[d] Universidade de Vigo, Applied Physics Department, School of Aeronautic and Space Engineering, As Lagoas s/n, Ourense, 32004, Spain
[e] Instituto de Física e Ciencias Aeroespaciais (IFCAE), Universidade de Vigo, As Lagoas s/n, Ourense, 32004, Spain

ARTICLE INFO

*Keywords:*
Mission analysis
Electric propulsion
Trajectory optimisation
Orbital insertion

ABSTRACT

Traditionally, space missions to outer planets have relied on large amounts of chemical propellant or flybys to achieve their objectives. This large mass consumption may be significantly reduced using electric propulsion (EP), since it allows for larger specific impulses. However, this improvement is counteracted by the lower thrust per power levels achievable with EP engines compared to chemical thrusters. Here we discuss how to find a balance for a purely solar EP (SEP) uncrewed mission to Mars. We present system engineering and mission analyses focused on the orbital mechanics. The result is the conceptual design of a realistic mission to Mars, in which any target orbit around Mars can be reached using solely present SEP technology. In particular, for a 2000 kg spacecraft propelled with a Hall effect thruster (HET), the interplanetary transfer can be performed in 363 days with less than 400 kg of fuel consumption, provided that the vehicle leaves the Earth orbit with a suitable specific energy that is attainable using current launchers. Subsequently, 300 kg of propellant are sufficient to allow for the planetary capture, plane change, and circularisation manoeuvres, finally inserting the spacecraft into a polar orbit of height between 300 km and 1000 km above the surface of Mars.

## 1. Introduction

Chemical propulsion has been the primary means of propelling spacecraft since the dawn of the Space Age. It can produce high thrust ($\sim 10^3$ N), but typically requires large propellant masses, ranging from 70% to 90% of the initial total mass [1].

Electric propulsion (EP) [2,3] is a more efficient and environmentally friendly alternative to chemical rockets. EP systems use electrically charged particles, such as ions or electrons, to generate thrust. For a given value of the available power, they produce lower levels of thrust ($\sim 5 \cdot 10^{-1}$ to $10^{-3}$ N) than chemical engines, but with much higher specific impulses ($I_{sp}$) [4], which correspond to a propellant mass fraction from 10% to 40% [1]. As a result, EP systems can carry more payload and equipment with the same total mass. For this reason, many space agencies are investing in EP technologies to reduce the cost and increase the efficiency of interplanetary missions, where the mass is a driven design factor.

Two classes of EP systems have been considered, depending on the method used for satisfying the power demand: solar EP (SEP) [5] and nuclear (NEP) [6]. SEP systems use photovoltaic cells to generate the power supply for the electric thruster. Their main advantages are the use of renewable energy and the reduced dry mass requirements for the electrical and power subsystem (EPS). Because these systems rely on Sun radiation, the power they can deliver decreases quadratically with the distance from the Sun as shown in Fig. 1. NEP systems use a nuclear reactor or a radioisotope thermoelectric generator (RTG), and are best suited to provide the required power for missions to the outer planets or beyond. Both SEP and NEP offer unique advantages for interplanetary missions, and the choice of the propulsion system depends on the specific mission requirements and constraints.

While chemical propulsion was traditionally used from the early days of space exploration, several interplanetary missions have already used EP. NASA's Dawn spacecraft [7] was launched in 2007 and used ion propulsion to travel to Vesta and Ceres asteroids. Another example is the Japanese Hayabusa2 spacecraft [8], which used ion engines to travel to and from Ryugu. The mission was successful in returning samples from the asteroid to the Earth in December 2020, demonstrating the capabilities of EP for deep space exploration.

EP technology is constantly improving and evolving, and future advancements are expected to significantly enhance its performance. One area of research is the development of EP systems achieving larger

* Corresponding author at: Aerospace Engineering Area, School of Aeronautic and Space Engineering, Universidade de Vigo, As Lagoas s/n, Ourense, 32004, Spain.
*E-mail addresses:* marco.casanova.alvarez@ext.esa.int, marco.casanova@uvigo.es (M. Casanova-Álvarez).

https://doi.org/10.1016/j.actaastro.2024.01.001
Received 8 August 2023; Received in revised form 14 December 2023; Accepted 2 January 2024
Available online 6 January 2024

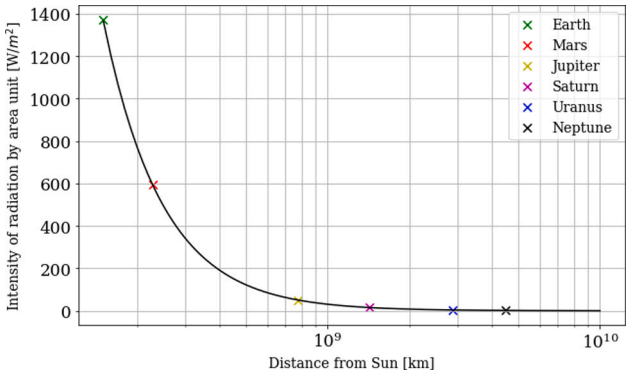


**Fig. 1.** Variation of sun intensity of radiation in the proximity of the Outer Planets of the Solar System.

values of the thrust and of the thrust to power ratio (T/P). The development of autonomous navigation and control systems could also allow electric-powered spacecraft to operate more independently, reducing the need for ground-based control and increasing the efficiency of space missions [9–12]. In summary, EP systems are expected to become more powerful, efficient, and versatile, making them a key component of future space missions to Mars and beyond.

There is limited previous work on system engineering analysis for EP missions to Mars. The requirements for a human mission with dry mass of 40 tonnes, including an analysis of the electric propulsion system, the power generation, and the sizing of the radiator for the thermal control, were explored in [6], relying on the possible future development of VASIMIR thrusters [13–15].

The possibility of fast transits to Mars, keeping aside the system engineering analysis of the spacecraft, were discussed in [16,17], relying on NEP with a power requirement at the level of 200 MW, which would hardly be feasible with present technology.

Twenty years ago, the benefits of employing various EP technologies were evaluated in [18]. The use of EP for Martian and lunar, cargo or crewed missions was studied in [19], providing an insight on how these technologies can overcome the challenges of delivering large amounts of mass (4 MT) when future pulse inductive thrusters (PIT) using up to 20 MW of power are available. An uncrewed SEP mission aimed at reaching the Martian moons, Deimos and Phobos, and returning samples back to Earth was presented in [20]. Finally, the feasibility of a SEP mission using large solar panels (75 $m^2$) and ion engines aimed at the exploration of Jupiter Trojan asteroids was explored in [21]. All of these studies demonstrated that, with the appropriate thruster and solar panel characteristics, EP is suitable for interplanetary missions.

Here, we demonstrate that SEP technologies that are already available in the market can be used for minimising the mass consumption of a mission to Mars, still keeping the duration of the interplanetary transfer below one year, and for efficiently performing the capture and plane change manoeuvres in the sphere of influence (SOI) of the planet. These results are obtained by designing optimisation algorithms that can also be used in any future mission concept, for any altitude and inclination of the target orbit around Mars. Moreover, the orbital simulations have been performed with an in-house n-body propagator that takes into account the gravitational effect of all the major massive bodies of the solar system, along with all the relevant perturbations, such as the solar radiation pressure, the aerodynamic drag of Mars' atmosphere and the planetary gravitational geopotential. This makes our results more accurate than those that we would have obtained using simple 2-body propagators as in the patched conics approximation [22, p. 417], the correction for the mass consumption being of the order of 10%.

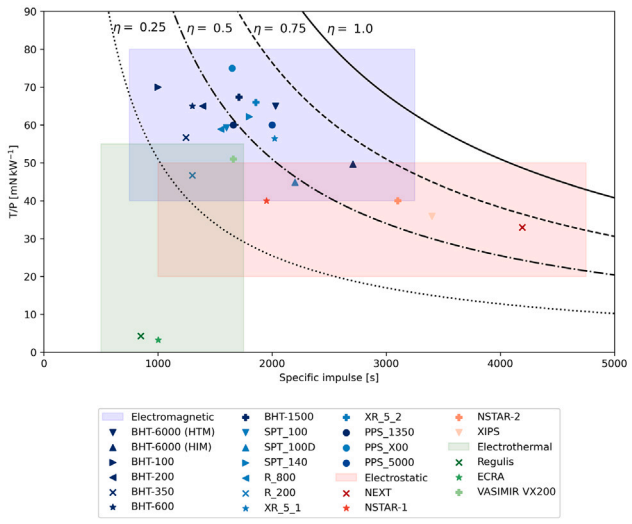


**Fig. 2.** Thrust per unit of power ratio (T/P) by specific impulse of each EP family and thruster.

## 2. State of the art for electric propulsion

Unlike traditional methods based on chemical reactions, EP systems use electric fields to accelerate charged particles (ions or electrons) and generate thrust. Different types of EP technologies, each with its own advantages and limitations, are available for choice, depending on the specific requirements of the mission:

- Electrothermal thrusters heat the propellant and create a pressure gradient that forces the propellant out of the nozzle. This is the case of the helicon plasma thruster (HPT) [23], the electron cyclotron resonance thruster (ECRT) [24], and the variable specific impulse magnetoplasma rocket (VASIMIR) [13–15].
- Electrostatic thrusters use electrostatic fields to accelerate the ions and force them out of the nozzle. This is the case of the gridded ion thrusters (GIT) [25] and electrospray thrusters [26].
- Electromagnetic thrusters use electrical currents and magnetic fields to accelerate the plasma. This is the case of the pulsed inductive thrusters (PIT) [27], the magnetoplasmadynamic thrusters (MPDT) [28], the applied field MPDT (AF-MPDT) [29], the pulsed plasma thrusters (PPT) [30], and the Hall effect thrusters (HET) [31].
- Thrusters using both the electrothermal effects and the electromagnetic acceleration [32].
- Thruster using the ambient radiation and plasma, such as electrodynamic tethers [33–35], or electric and magnetic sails [36, 37]. The main advantage of these technologies is that they are propellant-less.

Fig. 2 shows the thrust per power delivered to the propulsion system, the specific impulse and the overall system efficiency $\eta$ for a set of existing or future EP engines. Most of the electrothermal thrusters have low efficiencies and can be suitable for station-keeping manoeuvres in Earth's orbit, with the VASIMIR being the only proposal in this category that may meet the thrust and specific impulse requirements for supporting interplanetary missions in the future [13].

Electrostatic thrusters have a wider range of specific impulse, as compared to electrothermal devices, with efficiency reaching up to 75% for high specific impulses. Since HET can provide higher total thrust output with similar power consumption, they can be currently considered the most effective EP technology for interplanetary missions.

**Table 1**
Specifications of a selection of EP thrusters.

| Name | Technology | Thrust [mN] | Power [kW] | T/N [mN/kW] | I_sp [s] | Mass [kg] |
|---|---|---|---|---|---|---|
| BHT-100 | Hall effect | 7[a] | 0.1 | 70.00 | 1000 | 1.16 |
| BHT-200 | Hall effect | 13[a] | 0.2 | 65.00 | 1390 | 1 |
| BHT-350 | Hall effect | 17[a] | 0.3 | 56.67 | 1244 | 1.9 |
| BHT-600 | Hall effect | 39[a] | 0.6 | 65.00 | 1300 | 2.8 |
| BHT-1500 | Hall effect | 101 | 1.5 | 67.33 | 1710 | 7.1 |
| BHT-6000 (HTM) | Hall effect | 325 | 5 | 65.00 | 2029 | 12.5 |
| BHT-6000 (HIM) | Hall effect | 298 | 6 | 49.67 | 2708 | 12.5 |
| NEXT | Ion gridded | 236 | 7 | 33.71 | 4190 | 25.48 |
| NSTAR_1 | Ion gridded | 20[a] | 0.5 | 40.00 | 1950 | 26.94 |
| NSTAR_2 | Ion gridded | 92[a] | 2.3 | 40.00 | 3100 | 26.94 |
| Regulus | HPT | 1[a] | 0.8 | 1.25 | 850 | 2.5 |
| ECRA | ECRT | 0.98[a] | 0.3 | 3.27 | 1001 | 12 |
| VX200 | VASIMIR | 10 200 | 200 | 51.00 | 1660 | |
| SPT_100 | Hall effect | 80[a] | 1.35 | 59.26 | 1600 | 4 |
| SPT_100D | Hall effect | 112 | 2.5 | 44.80 | 2200 | 4.7 |
| SPT_140 | Hall effect | 280 | 4.5 | 62.22 | 1800 | 8.5 |
| R_800 | Hall effect | 53[a] | 0.9 | 58.89 | 1550 | 1.5 |
| R_200 | Hall effect | 14[a] | 0.3 | 46.67 | 1300 | 2 |
| XR_5_1 | Hall effect | 254 | 4.5 | 56.44 | 2020 | 12.3 |
| XR_5_2 | Hall effect | 132 | 2 | 66.00 | 1858 | 12.3 |
| PPS_1350 | Hall effect | 90[a] | 1.5 | 60.00 | 1660 | 5.3 |
| PPS_X0 | Hall effect | 75[a] | 1 | 75.00 | 1650 | 3.2 |
| PPS_5000 | Hall effect | 300 | 5 | 60.00 | 2000 | 12.3 |
| XIPS | Ion gridded | 79[a] | 2.2 | 35.91 | 3400 | 8.2 |

[a] Highlights the cases that do not attain the required thrust level ($\gtrsim 0.1N$) for this mission.

In particular, as we shall discuss in Section 4, a requisite for Mars capture is that the acceleration provided by the engine should be $\gtrsim 6 \times 10^{-5}$ m/s$^2$, which corresponds to a thrust level $T \gtrsim 0.1$ N for total mass around 1600 kg (the value that will be considered at the entrance of Mars' SOI). Such thrust level will also be shown to be sufficient for completing the interplanetary transfer in only one revolution around the sun, for a mass of 2000 kg after launch, as long as a first quasi-Hohmann delta v is provided by the launcher.

Table 1 shows the main specifications a large selection of thrusters. After discarding the engines that do not provide sufficient thrust, the selection was based on minimising the power requirements and maximising the specific impulse. The feasibility study focuses on using the characteristics of the BHT-6000 rocket [38] due to its reduced T/N ratio compared to the other suitable candidates. This engine can work in a high impulse mode (HIM) or in a high thrust mode (HTM) of operation. We chose the latter because of its smaller power consumption (5 kW, vs 6 kW for the HIM) and of its higher thrust (325 mN, vs 298 mN for the HIM). However, the methods for trajectory optimisation that we will develop for this example can also be applied to other engines that provide a sufficient thrust level for this mission, as long as their different characteristics are taken into account. This is the case for the ion gridded NEXT thruster or the SPT_140, the XR_5 and the PPS_5000 hall effect engines.

Table 2 shows the specifications of the BHT-6000 thruster in the selected HIM configuration. In the next sections, we shall demonstrate that this choice is already sufficient for performing all stages of a SEP mission to Mars with reduced mass consumption. Besides, our results and methods can also be applied to future thrusters that may provide higher efficiency and T/P.

## 3. System engineering design of a SEP spacecraft to Mars

This section presents a conceptual design of a SEP spacecraft to Mars in terms of following fields: mission and system requirements, concept of operations, functional architecture, and mass and power budgets. The main goal of this analysis is to demonstrate the feasibility of the mission proposed in this paper, both from the propulsion and the whole system points of view. The focal point is the orbital calculation of the spacecraft trajectory through the utilisation of SEP. However, the study of the electrical power subsystem (EPS) must not be undertaken in isolation; rather, it should be comprehensively examined in conjunction with the overall system engineering analysis.

**Table 2**
Standard specifications of BHT-6000 in high thrust mode (HTM).

| Characteristic | Value | Unit |
|---|---|---|
| Assembly mass | 12.5 | kg |
| Power consumption | 5 | kW |
| Voltage | 300 | V |
| Thrust | 325 | mN |
| Specific impulse | 2029 | s |
| Total impulse | 8.5 | MN-s |
| Propellants | Xenon, Krypton, Iodine | |
| Operating mode | Constant Exhaust Velocity (CEV) | |

### 3.1. Mission and system requirements

The mission requirements of a spacecraft propelled by a SEP system to Mars should consider the specific time constraints. As demonstrated in Section 4, a polar Martian orbit can be obtained for an initial mass of 2000 kg (after launch) accommodating a collection of payloads of 150 kg. Table 3 presents the mission and system requirements corresponding to these guidelines.

The scientific objectives of the mission will drive their requirements. Since an exhaustive scientific mission analysis is out of the scope of this work, we consider a science target set similar to that of previous projects, such as the European Space Agency's ExoMars mission [39]. Therefore, a set of instruments has been chosen for accomplishing the following objectives at all Mars latitudes: (a) characterising the atmosphere; (b) studying the hydrogen amount in the subsurface; and (c) studying the topography of the surface. The smallest set of instruments for performing these tasks could be: (1) A spectrometer that measures the sunlight reflected off the Martian atmosphere to identify gases, including methane, and map their location on the surface. (2) Spectrometers that measures the composition, structure, and dynamics of the Martian atmosphere. (3) A neutron detector that measures the amount of hydrogen in the Martian subsurface, which can help locate water and other volatiles. (4) A high-resolution camera that can image the Martian surface in 3D.

The resulting payload mass has been computed by comparing with that of the ExoMars set. Since the electric and power system (EPS) is over-dimensioned to satisfy the propulsion subsystem energy demand, the power available for the payload instruments is much higher than

**Table 3**
List of preliminary requirements for the mission and the system.

| | | Mission requirements |
|---|---|---|
| Req. ID | Req. title | Description |
| MR01 | Mission objective | The Mars Orbit Segment (MOS) shall generate and return scientific data from Mars surface. |
| MR02 | Mission coverage | MOS shall obtain scientific data from the complete atmosphere and surface of Mars during the mission life time |
| MR03 | Mission duration | The scientific lifetime of the mission shall be 5 years |
| MR04 | Observation distance to scientific target | The orbit periapsis shall be in the range of 300 to 400 km over the Martian surface |
| MR05 | Planetary protection regulation | MOS shall comply with the COSPAR's planetary protection policy, Category III |
| MR06 | Technology demonstration | A measuring system of the electric engine shall monitor the propulsion system performance during the complete mission |
| | | System requirements |
| SR01 | Mass budget | The maximum launch mass of MOS shall be 2000 kg |
| SR02 | Power budget | The maximum power of MOS shall be 25kW |
| SR03 | Propulsion power | The maximum power used for electrical propulsion shall be lower than 7 kW |
| SR04 | Interplanetary phase length | The mission interplanetary phase shall be completed in less than 2 years. |
| SR05 | Propellant mass | Propellant mass shall not exceed 1000 kg. |
| SR06 | Platform mass | Platform mass shall not exceed 1300 kg. |

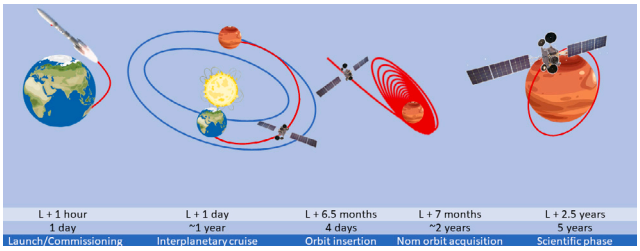


**Fig. 3.** ConOps of a SEP mission to Mars.

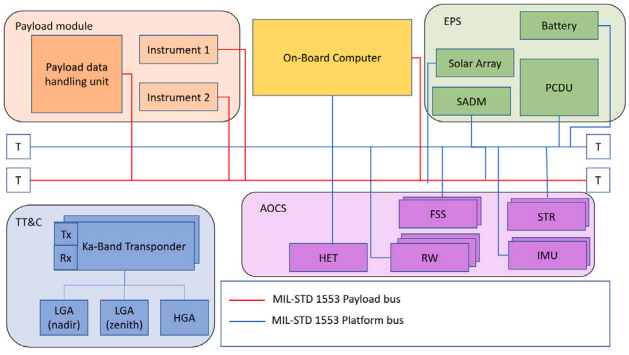


**Fig. 4.** Functional architecture of the spacecraft.

that used in ExoMars. Thus, the frequency and the duty cycle of the instruments can be increased, considering that, in parallel, the power available for the communication subsystem is also high once the EP is switched off. These factors are considered all along this system engineering analysis.

### 3.2. Concept of operations

Fig. 3 shows the concept of operations (ConOps) of the mission, which involves the following key phases, characterised by specific orbit manoeuvres, until the scientific phase orbit of the mission is reached:

**Launch and commissioning phase,** where the rocket injects the spacecraft into the desired escape orbit, initial telemetry is received and systems requirement compliance is checked (e.g. command capabilities are tested), and the solar array and antenna deployments take place. This phase should have a length of around one day. The launcher constraints and selection is presented in Section 4.

**Interplanetary phase,** in which the SEP performs a set of thrusting arcs, minimising the propellant consumption, in order to arrive to the martian SOI with the defined arrival asymptotic velocity. The length of this phase might vary depending on the weight factor of the variables to optimise-in this case, time of flight (ToF) and mass. In our selected transfer, the interplanetary phase has a duration of 362 days. Section 4.1 describes the obtained trajectory as well as the calculation methods used.

**Orbit insertion phase,** which consists of a 14 days manoeuvre starting when the spacecraft enters the SOI of Mars and finishing when the capture is obtained. Section 4.2 describes the optimal thrusting arcs that lead to this orbit result with minimal mass consumption.

**Nominal orbit acquisition phase,** with the manoeuvres to obtain the final orbit. In Sections 4.3 and 4.4, to demonstrate the capabilities of the mission, we choose a polar orbit with a periapsis altitude of 300 km and apoapsis altitude of 1000 km. This final orbit has been inspired by the optimal acquisition range of NOMAD's instrument [40,41]. This target is obtained with two subsequent manoeuvres, which are designed to optimise the propellant consumption. The first one achieves the desired inclination change in 10 days. The second one, which lowers and circularise the orbit, requires 2 years to be completed. During this period, the propulsion is activated only for short time arcs around the periapsis of the orbit.

**Scientific phase,** in which the payload is in acquisition mode performing the desired observations. Its duration depends on the payload requirements. A lifetime of 5 years is considered here for the mass calculations in order to counter act for orbit perturbations. This mission phase is characterised by its stable orbit, however, the instruments could also be switched on during the orbit circularisation (outside of eclipses and thrusting arcs).

### 3.3. Functional architecture

Fig. 4 shows the required subsystems and units for a mission to Mars, which were included in the mass and power estimations for our conceptual design.

As the purpose of this study is to illustrate the possibility to use a SEP system in martian orbit, the Electrical and Power Subsystem (EPS) will be mainly composed by photovoltaic panels, with a Solar Array Drive mechanism (SADM) for controlling their attitude, along with a

**Table 4**
Mass budget.

| S/C Mass Budget<br>Platform | | Mass [kg] | [%] |
|---|---|---|---|
| AOCS | | 40 | 3.75 |
| TT&C | | 50 | 4.69 |
| EPS | | 400 | 37.55 |
| DHS | | 50 | 4.69 |
| Structure | | 350 | 32.86 |
| Thermal | | 25 | 2.34 |
| Payload mass | | 150 | 14.08 |
| Dry Mass w/o System margin | | 1065 | |
| System margin | 20% | | |
| Dry Mass incl. System margin | | 1278 | |
| Xenon fuel mass | | 700 | |
| Xenon pressurant mass | | 20 | |
| Total Wet Mass | | 1998 | |

battery to feed the spacecraft during the eclipse periods. Besides, all equipment and devices require a Power Control and Distribution Unit.

The Attitude and Orbit Control subsystem (AOCS) will be integrated by inertial measurement units (IMUs), start trackers (STR), and fine sun sensors (FSS), as navigation tools, following the requirements of typical interplanetary missions [42,43]. Reaction wheels (RWs) will be chosen as attitude actuator, since they can provide the smooth orientation adjustments required in the mission with no mass consumption. As discussed in Section 2, the thruster is chosen to be the BHT-6000 HET engine.

The choice for telemetry tracking and control (TT&C) will be the recently developed Ka transponders [44–46], which allow for higher data transmission rates as compared to the X-band transmissions [47] used in past missions to Mars. It should be noticed that the power available for communications will be very large when propulsion subsystem is switched off.

As mentioned before, our purpose is the SEP feasibility validation, so we selected the payload instruments set for a typical space-observatory based on the previous mission ExoMars (exposed in Section 3.1).

### 3.4. Mass and power budgets

The conceptual design process implies to obtain a first guess of the basic budgets of the spacecraft. Table 4 presents the estimated mass budget. It takes into account all the spacecraft's systems for the mission. To conceptually size the solar panels and the battery, we required that they generate all the power needed by the electric engines, considering the sequence of thrusts and solar eclipses during the transfer and the manoeuvres around Mars. The periods of time when the engine is ON during a eclipse were obtained along the orbital simulations as explained in Section 4.5. The assumed parameters used to size the battery, as shown in Table 5, are average values based on different space-rated commercial products already employed by similar missions [48].

Table 6 presents the power budget, with the power consumption of the different subsystems during several operation modes. In the communication mode, the HGA and Ka-transponders are ON; in the propulsion mode, the HET thruster is active; and in the eclipse-propulsion mode, the thruster and the heaters are ON during a solar eclipse. The maximum power consumed in the worst scenario after applying margins is roughly 6 kW, which has been used to estimate the required solar array area, 30 $m^2$, and its corresponding mass.

**Table 5**
Power assumptions.

| Variable | Value | Unit |
|---|---|---|
| Capacitance of battery | 14 | A hour |
| Solar cell degradation per year | 3.75 | % |
| Solar cell efficiency | 47 | % |
| Depth of battery discharge | 20 | % |
| Transmission efficiency | 0.9 | |
| Battery cell capacity | 1.5 | Amp/hour |
| Specific performance of solar array | 25 | W/kg |
| Ratio of battery capacity to mass | 133 | W hr/kg |

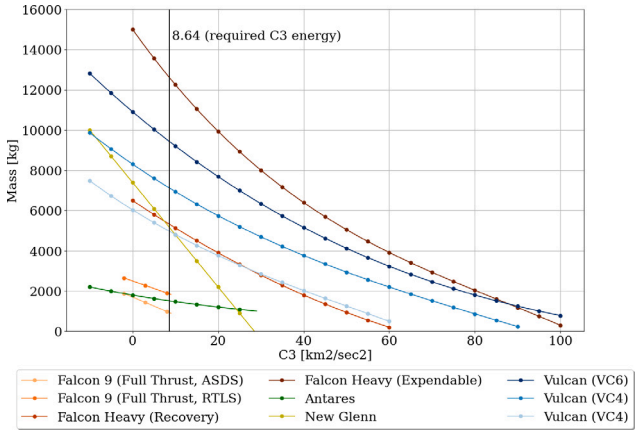


**Fig. 5.** Launchers C3 capability by cargo mass. Data obtained from [49].

## 4. Orbital analysis

In this section, we show how the spacecraft designed in Section 3 can be sent to the target orbit around Mars by only using its SEP system, after the initial Delta v applied at launch. This transfer is performed in four phases or manoeuvres, corresponding to the interplanetary trajectory, the capture, the plane change, and the circularisation. For all parts of the mission, we perform the orbital computations using in-house n-body propagator and implementing optimisation strategies designed to minimise the propellant consumption within reasonable constraints about the time of flight. We first discuss the optimisation of each stage of the trajectory. The results of the global optimisation for the entire mission are then presented in Section 4.5, and are used to obtain the most convenient initial and final conditions at each intermediate stage.

Current launchers are able to provide, for the considered mass of 2000 kg, a characteristic specific energy, $C_3$, up to 140 $km^2/s^2$, which is sufficient to reach Saturn with a direct transfer, as shown in Fig. 5. For our mission to Mars, we selected $C_3 = 8.64$ $km^2/s^2$ based on optimisation iterations. A fraction of it, namely $C_3^{\text{orthogonal}} \simeq 1.12$ $km^2/s^2$, is used for changing the inclination of the trajectory and attain the orbital plane of Mars. The component in the orbital plane, $C_3^{\text{coplanar}} \simeq 7.52$ $km^2/s^2$, is smaller than that required to perform the first burn of an ideal coplanar Hohmann chemical manoeuvre between the Earth and Mars distances, $C_3^{\text{Hohmann}} = 8.41$ $km^2/s^2$. This difference is due the fact that, unlike for a pure Hohmann transfer, the EP engine has to be turned on for a long arc before the rendezvous, so that the apoaxis of the osculating transfer ellipse is continuously raised during the manoeuvre. Therefore the smaller value of $C_3^{\text{coplanar}}$, as compared with $C_3^{\text{Hohmann}}$, allows us for reaching a nearly parabolic rendezvous with Mars avoiding any deceleration during the interplanetary phase, thus minimising the propellant consumption. As the required departure energy is provided by the launcher, there is no need of consumption of Xenon prior to the interplanetary phase.

**Table 6**
Power budget. Mission phases acronyms: interplanetary phase, IP; capture phase, CP; plane change phase, PCP; transfer-to-lower-orbit phase, TtLOP; Nominal phase, NP.

| Power consumption assumption | | | Science mode: full power | Science mode: medium power | Comms mode | Propulsion mode | Eclipse and Propulsion mode |
|---|---|---|---|---|---|---|---|
| Mission phases | | | NP | IP, TtLOP, NP | All phases | IP, CP, PCP, and TtLOP | CP, TtLOP, and NP |
| Subsystem | Status | Margin | Consumption [W] | Consumption [W] | Consumption [W] | Consumption [W] | Consumption [W] |
| OBDH | ON | 20% | 5.000 | 5.000 | 5.000 | 5.000 | 5.000 |
| EPS | ON | 20% | 10.000 | 10.000 | 10.000 | 10.000 | 10.000 |
| COM | ON | 20% | 0.000 | 0.000 | 700 | 0.000 | 0.000 |
| AOCS | ON | 20% | 15.000 | 15.000 | 15.000 | 5,015.000 | 5,015.000 |
| THS | ON | 20% | 0.000 | 0.000 | 0.000 | 0.000 | 50.000 |
| STRUCT | ON | 20% | 0.000 | 0.000 | 0.000 | 0.000 | 0.000 |
| PAYLOAD | ON | 20% | 700 | 350 | 0.000 | 0.000 | 0.000 |
| Total power consumption | | | 730.000 | 380.000 | 730.000 | 5,030.000 | 5,080.000 |
| Power with margin (+20%) | | | **876.000** | **456.000** | **876.000** | **6,036.000** | **6,096.000** |

### 4.1. Interplanetary phase

Due to the small value of the thrust, EP requires thrusting arcs to obtain the desired orbital changes, in contrast with chemical propulsion, whose effect can often been approximated as instantaneous $\Delta v$. An estimate can be obtained by noticing that the interplanetary transfer should raise the specific energy of the spacecraft from $\varepsilon^{\text{in}} \simeq \varepsilon_{\text{launcher}} - \frac{\mu_{\text{sun}}}{2D_{Earth}}$ (where $\mu_{\text{sun}} \simeq 1.3 \times 10^{20}$ m$^3$/s$^2$ is the standard gravitational parameter of the sun and $\varepsilon_{\text{launcher}}$ is the net contribution of the launcher), corresponding to an orbit at the distance $D_{\text{Earth}} \simeq 1$ AU from the sun, to the level $\varepsilon^{\text{fin}} \simeq -\frac{\mu_{\text{sun}}}{2D_{Mars}}$, corresponding to the distance $D_{\text{Mars}} \simeq 1.5$ AU. This change can be obtained by turning on the thrust $T$ in the direction of the velocity along an arc of length $\Delta l$, provided $T\Delta l \simeq \bar{m}\left(\varepsilon_{\text{launcher}} + \frac{\mu_{\text{sun}}}{2D_{Earth}} - \frac{\mu_{\text{sun}}}{2D_{Mars}}\right)$, where $\bar{m}$ is the average mass during the manoeuvre. If we require that the transfer is completed in a single revolution around the sun, so that $\Delta l \lesssim 2\pi D_{Mars}$, and neglect the contribution of the launcher $\varepsilon_{\text{launcher}}$, then the average acceleration should be at least of the order $\frac{T}{\bar{m}} \gtrsim 4.2{\times}10^{-4}$ m/s$^2$. For a vehicle of mass $\bar{m} \sim 2000$ kg, this would require a thrust level of the order of $T \gtrsim 0.8$ N. This limit may be relaxed by allowing for more revolutions around the sun before the rendezvous with Mars, with the resulting larger cost in time and fuel consumption. A better strategy is using the launcher for providing a significant part of the energy of the transfer, by inserting the vehicle in a quasi-Hohmann transfer ellipse as discussed above, with $C_3^{\text{coplanar}} \simeq 7.52$ km$^2$/s$^2$. With this value, the average acceleration from the EP for achieving the rendezvous with Mars should be at least of the order of $\frac{T}{\bar{m}} \gtrsim 4.2 \times 10^{-5}$ m/s$^2$. In this case, for a vehicle of mass $\bar{m} \sim 2000$ kg, this would require $T \gtrsim 0.08$ N. Since the BHT-6000 engine can provide a significantly larger thrust level, we can expect that there will be room for further trajectory optimisation.

In fact, the accurate analysis that we present below confirms this expectation. We integrated the full mass-dependent equations of motion, including the continuous EP acceleration, implementing special optimisation procedures to minimise the mass usage. In particular, we used ESA's pykep and pygmo libraries [50–52] for parallel global multi-objective optimisation. Table 7 shows the initial conditions as well as the spacecraft configuration variables used to assess the best thrusting strategy for the interplanetary phase.

A weight factor has been used to balance the importance assigned to each of the two objectives of the optimisation, the time of flight (ToF) along the interplanetary transfer manoeuvre and the mass consumption. Giving priority to the minimisation of the latter, the weight of mass objective relative to the total optimisation has been set to 0.999, which also corresponds with the Pareto efficiency [53].

With these inputs, an optimal trajectory has been found with the characteristics defined in Table 8. When studying the orbit resonances between the Earth and Mars, there are optimal launch windows every 2 years, depending on the number of revolutions around the Sun that are accepted before reaching the target. Since the reduction in mass consumption with additional revolutions is small, we considered a maximum ToF of 365 days. As a result, we obtained an optimal ToF of 363 days, which is roughly a 40% longer time than for the ideal case of a chemical-propelled Hohmann manoeuvre. Fig. 6 shows the selected orbit, highlighting in red the thrusting arcs.

**Table 7**
Interplanetary optimisation inputs.

| Variable | Value | Unit |
|---|---|---|
| Launch Mass | 2000 | [kg] |
| Mass at Mars' SOI | 1500 | [kg] |
| Thrust | 0.3 | [N] |
| $I_{sp}$ | 2029 | [s] |
| Launch window | [2030-01-01, 2040-01-01] | |
| Time of flight (ToF) | [200, 365] | [days] |
| Departure infinity velocity | 2.94 | [km/s] |
| Arrival infinity velocity | 0.001 | [km/s] |
| Weight factor mass | 0.999 | |

**Table 8**
Interplanetary optimisation outputs.

| Variable | Value | Unit |
|---|---|---|
| Launch Epoch | 2031-01-31 06:38 | |
| Arrival Epoch | 2032-01-29 05:14 | |
| Mass at Mars' SOI | 1616 | [kg] |
| Time of flight (ToF) | 362.94 | [days] |

Fig. 7 shows the thrust profiles during the transfer. The trajectory optimisation used different normalised thrust levels to provide variable thrust depending on the orbit requirement. In all the figures of this section, the time elapsed since the launch epoch, as measured in days, is called Days of Mission (DoMs).

The evolution of the mass consumption during this phase of the mission can be seen in Fig. 8. The resulting final mass of the spacecraft will be used as the starting value for the capture and plane change manoeuvres in the martian SOI.

### 4.2. Capture phase

Hereafter, we use the two-body approximation in order to design thrusting strategies for minimising the propellant consumption during the capture, plane change, and circularisation manoeuvres. This approach allows to reduce the complexity of the control laws up and make them feasible for implementation in an on-board AOCS. However, we also implemented the resulting optimisation methods in the full multibody and multi-perturbation propagator to obtain our complete numerical results, and checked that they remain effective

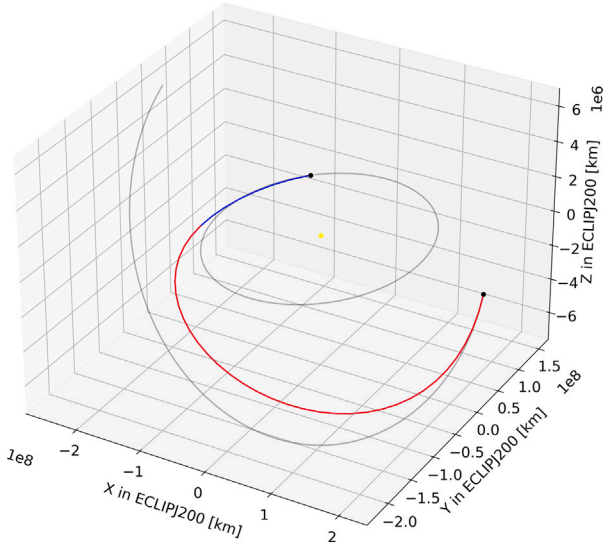


**Fig. 6.** Interplanetary transfer trajectory in ECLIPJ2000 inertial reference frame. The arcs in which the thrust is ON and OFF are highlighted in red and blue colours, respectively. The black dots correspond to the departure and arrival positions of the Earth and Mars. The orbits of the two planets during the transfer are displayed in grey.

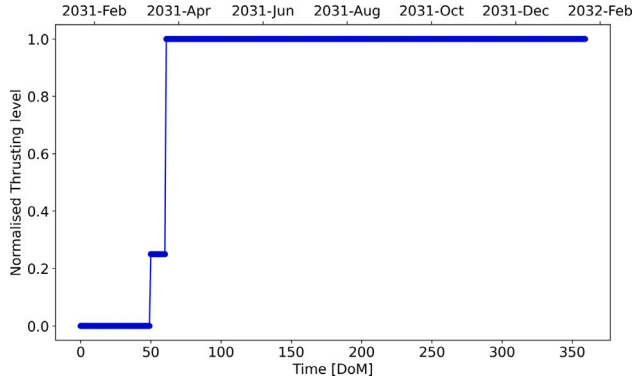


**Fig. 7.** Normalised thrust level during interplanetary course.

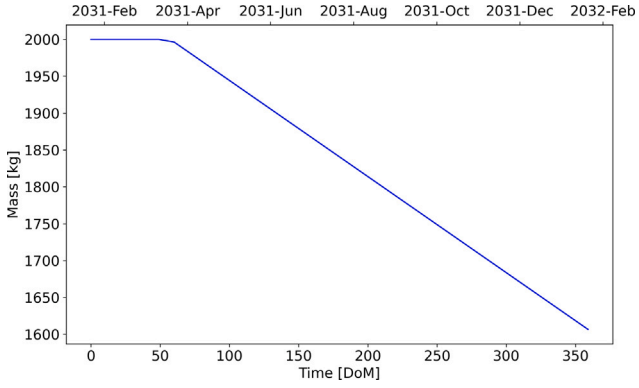


**Fig. 8.** Mass consumption during interplanetary course.

control laws for minimising the fuel consumption even beyond the two body approximation.

We assume that the space vehicle enters the SOI of Mars in a hyperbolic or parabolic orbit with eccentricity $e^{\text{in}} \geq 1$, and projected distance at periapsis $r_p^{\text{in}}$. These parameters describe the incoming trajectory in the two body approximation, as observed in an inertial frame centred in Mars. They are related to the asymptotic arrival velocity of the vehicle $v_\infty$, so that $e^{\text{in}} = 1 + \frac{r_p^{\text{in}} v_\infty^2}{\mu}$. Since $v_\infty$ is given by the interplanetary transfer, the shape of the hyperbolic trajectory during the flyby is determined by the choice of the impact distance $r_p^{\text{in}}$.

At a convenient instant $t^{\text{in}}$, whose optimal value will be determined below, the engines are turned on, applying a thrust force $\mathbf{T}$. Within the two body approximation, the time evolution of the vehicle mass $m(t)$ and of its position and velocity vectors, $\mathbf{r}(t)$ and $\mathbf{v}(t)$, as observed in the Mars-centred inertial frame, can then be obtained by integrating the following system of ordinary differential equations,

$$\begin{aligned}
\dot{\mathbf{r}} &= \mathbf{v}, \\
\dot{\mathbf{v}} &= -\mu \frac{\mathbf{r}}{r^3} + \frac{\mathbf{T}}{m}, \\
\dot{m} &= -\frac{T}{c},
\end{aligned} \tag{1}$$

where $\mu$ is Mars standard gravitational parameter, $T = |\mathbf{T}|$, and $c$ is the effective exhaust velocity of the fuel [22, p. 299–365 and p. 619–649]. In order to maximise the rate of orbital energy reduction for the capture manoeuvre, the thrust will be chosen to be antiparallel to the velocity vector, so that $\mathbf{T} = -T\frac{\mathbf{v}}{v}$.

The capture will be obtained if $R^{\min} < r < R^{\text{SOI}}$ for all time $t > t^{\text{in}}$, where the minimum distance $R^{\min}$ can be chosen depending on the mission requirements (in our case the ones covered in Section 3.1), for instance it may be the radius of Mars including its atmosphere. This also implies that the orbit has to become elliptic after the manoeuvre, corresponding to eccentricity $e^{\text{fin}} < 1$ and final distance at apoapsis $r_a^{\text{fin}} < R^{\text{SOI}}$.

In this case, the evolution of the osculating orbital elements is given by Gauss variational equations [22, P.651–720],

$$\begin{aligned}
\dot{h} &= -\frac{h}{v}\frac{T}{m}, \\
\dot{e} &= -\frac{2}{v}(e + \cos\theta)\frac{T}{m}, \\
\dot{\Omega} &= 0, \\
\dot{i} &= 0, \\
\dot{\omega} &= -\frac{2}{ev}\sin\theta\frac{T}{m}, \\
\dot{\theta} &= \frac{h}{r^2} + \frac{2}{ev}\sin\theta\frac{T}{m}, \\
\dot{m} &= -\frac{T}{c}.
\end{aligned} \tag{2}$$

Therefore, this thrust continuously modifies the osculating eccentricity $e$ and specific angular momentum $h$ of the trajectory without changing the orbital plane, which is described by constant angles $i$ and $\Omega$. Eqs. (2) also imply that the value of the projected distance at periapsis $r_p = \frac{h^2}{\mu(1+e)}$ decreases during the approach manoeuvre, with a relative change per unit time given by

$$\frac{\dot{r}_p}{r_p} = -\frac{2}{v}\frac{(1-\cos\theta)}{1+e}\frac{T}{m}. \tag{3}$$

If the engines are turned on far from the periapsis, a large initial impact parameter $r_p^{\text{in}}$, possibly of the order of $R^{\text{SOI}}$, can be required in order to keep $r_p > R^{\min}$ for all time. However, if the propulsion is only activated for $r$ close to $r_p^{\text{in}}$, so that $\cos\theta \sim 1$, then $\dot{r}_p$ is very small and $r_p^{\text{in}}$ can be chosen to be of the order of the periapsis distance of the target orbit.

The consequences of the capture condition, $r < R^{\text{SOI}}$ for all time $t > t^{\text{in}}$, can also be inspected by using the energy equation, which can be obtained e.g. from Eqs. (2) taking into account the expressions $r = 1/(1 + e\cos\theta)$ and $v = \frac{\mu}{h}\sqrt{1 + e^2 + 2e\cos\theta}$, so that [22, p.299–365],

$$\frac{\mathrm{d}}{\mathrm{d}t}\left(\frac{v^2}{2} - \frac{\mu}{r}\right) = -\frac{T}{m}v. \tag{4}$$

Assuming that the engine produces constant thrust $T$ for the duration of the manoeuvre $t^{\text{in}} \leq t \leq t^{\text{fin}}$, the integration of the last line in Eqs. (1) gives $m = m^{\text{in}} - \frac{T}{c}(t - t^{\text{in}})$. By relating the specific energies of the final ellipse and the incoming hyperbola to their corresponding

eccentricities and periapsis distances, and then integrating Equation (4) over time while reversing the signs, we arrive at

$$\varepsilon \equiv \frac{\mu}{r_p^{\rm fin} + r_a^{\rm fin}} + \frac{v_\infty^2}{2} = T \int_{t^{\rm in}}^{t^{\rm fin}} \frac{v \mathrm{d}t}{m^{\rm in} - \frac{T}{c}(t - t^{\rm in})}, \tag{5}$$

where we have defined the quantity $\varepsilon$, which is a measure of the specific energy provided by the propulsion during the manoeuvre.

Eq. (5) can be used to obtain an estimate of the minimum acceleration level required for obtaining the capture before leaving Mars' SOI. The limiting case corresponds to $r_a^{\rm fin} \simeq R^{\rm SOI}$ and an almost parabolic rendezvous, so that $v_\infty$ can be neglected. If $\int v dt \equiv 2bR^{\rm SOI}$, with $b \simeq \mathcal{O}(1)$, is the length of the thrusting arc, which has to be completed before reaching the apoaxis, we obtain the approximation $\left(\frac{T}{\bar{m}}\right)_{\rm limit} \simeq \frac{\mu}{2b(R^{\rm SOI})^2} \simeq 6 \times 10^{-5} \mathrm{m/s^2}$, where $\bar{m}$ is the average value of the mass during the manoeuvre. For an initial mass of 1600 kg, this corresponds to the requirement that the thrust $T$ should be of the order of 0.1 $N$ or larger. Since the BHT-6000 engines that we chose in Section 2 provides a significantly higher level for $T$, there is room for optimising the trajectory by choosing the instant of ignition and the initial impact parameter $r_p^{\rm in}$ of the incoming hyperbola, as discussed below.

According to Eq. (4), the rate of energy depletion is proportional to the velocity $v$, which is larger for smaller values of $r$. Therefore it is convenient to turn on the engines as close as possible to the periapsis, ensuring that the capture is still obtained. An optimal value $-\Theta$ of the true anomaly along the incoming hyperbola for starting the propulsion can be determined by the following iterative procedure which is summarised in Fig. 9.

1. Choose the desired value $r_a^{\rm fin}$ of the captured orbit, for instance $r_a^{\rm fin} = R^{\rm SOI}$.
2. Define the impact parameter $r_p^{\rm in}$ of the incoming hyperbola in the orbit plane. Assuming a given value $v_\infty$ for the arrival velocity, which is determined by the interplanetary transfer, $e^{\rm in}$ can be expressed in terms of $r_p^{\rm in}$, as $e^{\rm in} = 1 + \frac{r_p^{\rm in} v_\infty^2}{\mu}$. Because $r_p$ decreases during the manoeuvre, such $r_p^{\rm in}$ should be large enough as to prevent $r_p^{\rm in}$ from falling below $R^{\rm min}$. This condition will be tested *a posteriori* (see point 8 below).
3. Make a first guess $r_p^{\rm fin,0}$ for $r_p^{\rm fin}$. The actual value of $r_p^{\rm fin}$ will be obtained later from the numerical integration of Eqs. (1), and it has to be larger than $R^{\rm min}$ and smaller than $r_p^{\rm in}$. Therefore, a reasonable first guess can be the average value $r_p^{\rm fin,0} = \frac{1}{2}(r_p^{\rm in} + R^{\rm min})$.
4. Compute the specific energy $\varepsilon$ using the definition in Eq. (5). The input value $r_p^{\rm fin,i}$ for $r_p^{\rm fin}$ will be that given by the previous step, which is point 3 (for the first iteration, corresponding to $i = 0$) or point 7 (for the subsequent iterations).
5. Use Eq. (5) to compute the approximate length of the trajectory during the time span in which the engine is turned on,

$$\int_{t^{\rm in}}^{t^{\rm fin}} v \mathrm{d}t \simeq \varepsilon \frac{\bar{m}}{T}, \tag{6}$$

using the initial mass as an estimate for $\bar{m}$, which is a good approximation if the fuel consumption during the capture is a small fraction of the total mass of the vehicle.
6. Equate the result of the previous step, Eq. (6), with the length of a parabolic orbit of periapsis distance $\bar{r}_p \simeq (r_p^{\rm in} + r_p^{\rm fin,i})/2$. Taking into account the expressions for the velocity and for $\dot{\theta} = \frac{h}{r^2} = \frac{\mu^2(1+e\cos\theta)^2}{h^3}$. Then we obtain

$$\begin{aligned} \int_{t^{\rm in}}^{t^{\rm fin}} v \mathrm{d}t &= \int_{-\Theta}^{\Theta} \frac{h^2}{\mu} \frac{\sqrt{1+e^2+2e\cos\theta}}{(1+e\cos\theta)^2} d\theta \Big|_{e\to 1} \\ &\simeq 4\sqrt{2}\,\bar{r}_p \frac{\cos\frac{\Theta}{2}\left[\sin\frac{\Theta}{2} + \cos^2\frac{\Theta}{2}\arctan(\sin\frac{\Theta}{2})\right]}{(\cos\Theta+1)^{3/2}}, \end{aligned} \tag{7}$$

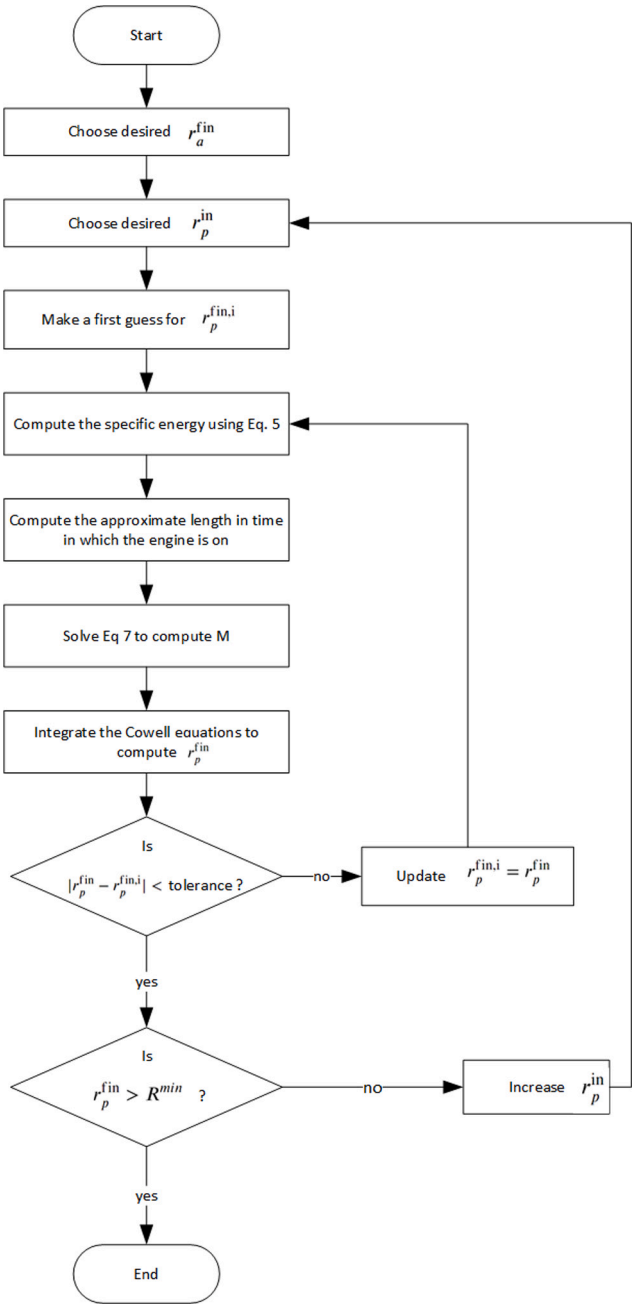


**Fig. 9.** Algorithm used for insertion optimisation.

where $h$ is the osculating specific angular momentum, corresponding to a projected distance at periapsis $r_p = \frac{h^2}{2\mu}$ for the parabolic orbit. This approximation can be expected to be accurate when the initial and final eccentricities are slightly larger and smaller than 1, respectively, so that their average value $\bar{e}$ can be taken to be 1, and when the thrust is large enough as to allow for $r_p^{\rm in}$ and $r_p^{\rm fin}$ having the same order of magnitude. By equating the last term with $\varepsilon \frac{\bar{m}}{T}$, a value of the true anomaly $-\Theta$ along the incoming hyperbola at which the engines have to be turned on can be obtained using a root finding method, such as bisection (see e.g. the implementation in [54]). The engines will then be turned off when the osculating value of $r_a$ reaches the desired value, $r_a^{\rm fin}$.
7. Numerically integrate the full Cowell equations with the full multibody propagator, which also includes the effect of the sun,

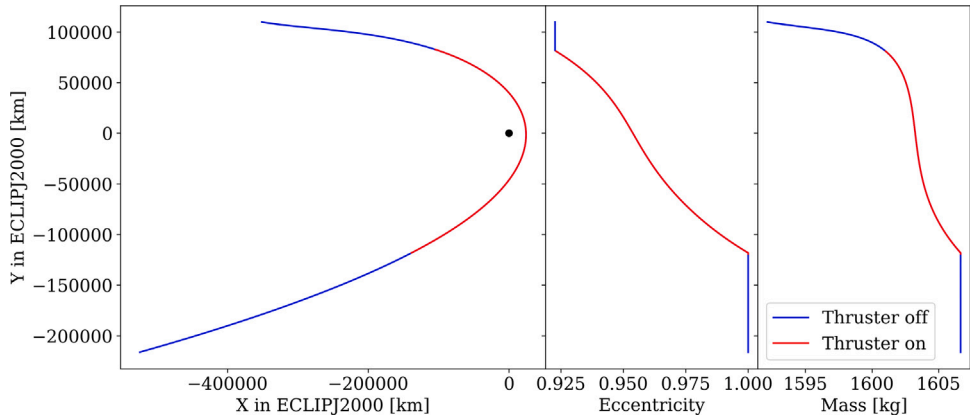


**Fig. 10.** Evolution during the capture manoeuvre, with the thrusting arc highlighted in red colour. The trajectory (left) is represented in an ECLIPJ2000 reference frame centred in Mars. The eccentricity (centre) decreases during the manoeuvre, until a stable orbit is reached, at expenses of mass consumption (right). The movement proceeds to increasing values of $Y$.

and with the thrust activated when $r < r^{\text{in}}(\Theta) = \frac{(1+e^{\text{in}})r_p^{\text{in}}}{1+e^{\text{in}}\cos\Theta}$, and compare the result for the final osculating distance at periapsis, $r_p^{\text{fin}}$, with the last value $r_p^{\text{fin,i}}$ used in the previous steps. If the absolute value of such difference is larger than a certain tolerance, then $r_p^{\text{fin}}$ will be used instead of $r_p^{\text{fin,i}}$ for a new iteration through steps 4 to 7.

8. The final value for $r_p^{\text{fin}}$, as obtained after the propagation when the engines are turned on at the point $\Theta_{\text{opt}}$ determined above, has to be larger than $R^{\text{min}}$. Otherwise, the initial value of $r_p^{\text{in}}$ has to be increased.
9. Given the initial eccentricity, a scan over the values of $r_p^{\text{in}}$ will be performed, implementing the previous steps for each of them. This procedure allows for choosing the most convenient value of $r_p^{\text{in}}$ depending on the mission requirements. Lower values of $r_p^{\text{in}}$ imply smaller fuel consumption for the capture manoeuvre. However, $r_p^{\text{in}}$ has to be larger than the minimum distance, and it should also be large enough as to allow for the subsequent manoeuvres. Therefore, the final choice has to be done considering the actual target orbit, corresponding to the requirements of Section 3.1.

Taking the state vector and the mass properties of the spacecraft after reaching the SOI of Mars (as per previous Section) as initial conditions, we used this algorithm to optimise the orbital insertion by thrusting only in the optimal arc of the orbit. Fig. 10 shows the geometry of the resulting trajectory, with the thrusting arc indicated in red. The evolution of the osculating eccentricity and of the mass is also shown, with the convention that the plotted values correspond to the times in which the position of the vertical coordinate $Y$ is reached.

### 4.3. Plane change manoeuvre

Once the vehicle has been captured, a plane change manoeuvre can be performed by applying propulsion in the direction of the angular momentum vector. In this case, the evolution of the osculating orbital elements is described by Gauss variational equations [22, p. 651–720],

$$\dot{h} = 0$$
$$\dot{e} = 0$$
$$\dot{\Omega} = \frac{r}{h\sin i}\sin(\omega+\theta)\frac{T}{m} = \frac{h}{\mu}\frac{\sin(\omega+\theta)}{(1+e\cos\theta)\sin i}\frac{T}{m}$$
$$\dot{i} = \frac{r}{h}\cos(\omega+\theta)\frac{T}{m} = \frac{h}{\mu}\frac{\cos(\omega+\theta)}{(1+e\cos\theta)}\frac{T}{m}$$
$$\dot{\omega} = -\frac{r\sin(\omega+\theta)}{h\tan i}\frac{T}{m} = -\frac{h}{\mu}\frac{\sin(\omega+\theta)}{(1+e\cos\theta)\tan i}\frac{T}{m}$$
$$\dot{\theta} = \frac{h}{r^2}$$
$$\dot{m} = -\frac{T}{c}. \tag{8}$$

Here, $T$ is defined as the unique component of the thrust along the unit orthogonal vector $\mathbf{W} = \mathbf{h}/h$, where $\mathbf{h} = \mathbf{r}\times\mathbf{v}$. In other words, $\mathbf{T} = T\mathbf{W}$, and $T$ is taken to be positive/negative if it is parallel/antiparallel to the angular momentum.

According to Eqs. (8), this thrust does not modify the osculating $e$ and $h$ of the trajectory, but it can produce a change of the orbital plane. However, the variation of the inclination $i$, of the right ascension of the ascending node $\Omega$, and of the argument of the perigee $\omega$ are modulated by trigonometric functions that change sign twice during a period of the orbit. In particular, the sign change of $\dot{i}$ occurs when the vehicle crosses the line of nodes. Therefore in a manoeuvre aiming at modifying the inclination, the propulsion should be either turned off, or switched to the opposite direction when the line of nodes is crossed. The first possibility is probably easier to be implemented in practice.

In order to optimise the efficiency of the manoeuvre and minimise the fuel consumption, it can be convenient to switch on the engines only when $\dot{i}$ is as large as possible, besides having the correct sign. The best strategy is to perform the plane change manoeuvre before lowering and circularising the orbit, when the values of $h$ and $e$ are larger. This is an advantage because $\dot{i}$ is proportional to $h$, and because of the $1+e\cos\theta$ factor in the denominators of Eq. (8), which can be large for $e$ close to 1.

In each turn, the maximum positive and minimum negative values of $\dot{i}$ are attained when the osculating true anomaly is $\theta_+ = -\omega - \arcsin(e\sin\omega)$ and $\theta_- = \pi - \omega + \arcsin(e\sin\omega)$, respectively, both values being defined within an additional multiple of $2\pi$. The most efficient option is to turn on the engine for $\theta$ around $\theta_m = \theta_+$ or $\theta_m = \theta_-$, depending on which case corresponds to the maximum value of $|\dot{i}|$. For the sake of consistently increasing the inclination, the propulsion has to be directed along $\mathbf{W}$ around $\theta_+$ or along $-\mathbf{W}$ around $\theta_-$, respectively. The opposite choice can be used for decreasing the inclination. This alignment has to be obtained by continuously controlling the attitude of the vehicle. Moreover, in order to maximise the effect, it is convenient to choose a small angular width $\delta$ of the region in which the engine is turned on. This will also ensure that the osculating $\omega$ does not vary significantly during each ignition spot.

This strategy must be modified for values of inclination close to 0, since in this case the node line is not defined. In this limit, the ignition can be activated around the apoapsis to kickstart the process, e.g. for $r > 0.9\,r_a$, choosing the $-\mathbf{W}$ or $+\mathbf{W}$ direction in order to increase or decrease the inclination, respectively.

We can estimate the variation $\Delta i_{\text{turn}}$ of the inclination per turn during such plane change manoeuvre as

$$\Delta i_{\text{turn}} \approx \frac{r_a}{h}\frac{T}{\bar{m}}\frac{r_a^2}{h}\Delta\theta \simeq \frac{r_a^3}{\mu r_p}\frac{T}{\bar{m}}\delta \tag{9}$$

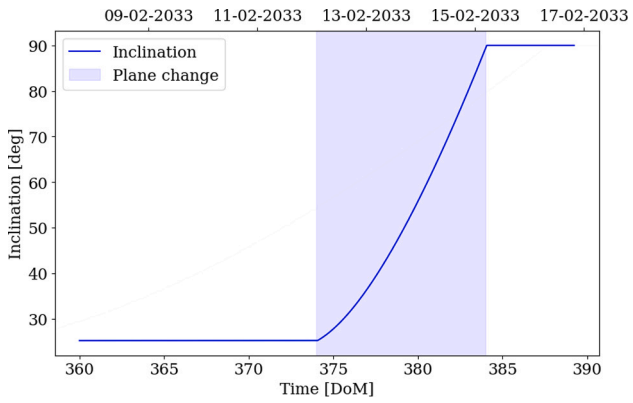


**Fig. 11.** Evolution of the inclination during the plane change manoeuvre.

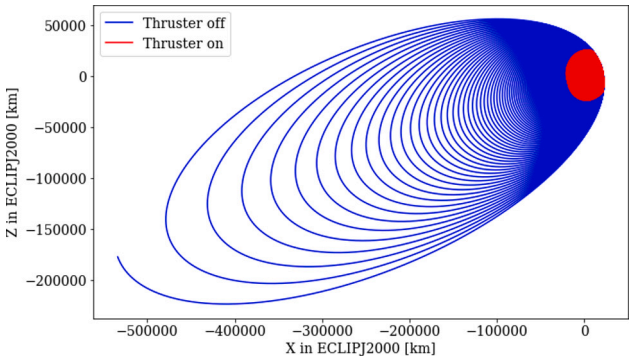


**Fig. 12.** Trajectory during the circularisation manoeuvre, with the thrusting arcs highlighted in red colour, as represented in an ECLIPJ2000 reference frame centred in Mars. (For interpretation of the references to colour in this figure legend, the reader is referred to the web version of this article.)

where we have assumed that the propulsion is active for $\theta_m - \delta < \theta < \theta_m + \delta$, and that $e$ is close to 1, so that $h^2 = \mu r_p(1+e) \simeq 2\mu r_p$. For example, in the case of Mars, with an acceleration of $\frac{T}{\bar{m}} \simeq 2 \times 10^{-7}$ km/$s^2$, and with $r_a \simeq R^{\text{SOI}}$ after the capture, the best choice for $r_p$ is around $r_p^{\text{in}} \simeq 0.045 R^{\text{SOI}}$, so that $\Delta i_{\text{turn}} \approx 35\,\delta$. In this case, a mere $\delta \sim 3°$ angular width of the region in which the propulsion is applied is sufficient to achieve a 90° degree inclination change in just one turn. Yet, a few days are required to cover such angle around the distance $r_a \simeq R^{\text{SOI}}$.

Fig. 11 shows the inclination change performed during the manoeuvre, as computed with the full multibody propagator. As expected, the polar orbit is reached after 10 days, with a fuel consumption of 12 kilograms. The initial value is the inclination of Mars orbital plane as seen from its equatorial reference frame.

### 4.4. Transfer to lower orbit

The target orbit is usually designed depending on the scope of the mission and the optimal operation regime of the instrumentation. In general, we assume that this corresponds to requiring $r_p^{\text{target}} < r < r_a^{\text{target}}$, so that $r_p^{\text{target}} > R^{\min}$ and $r_a^{\text{target}} < R^{\text{SOI}}$ are the periapsis and apoapsis distances of the desired elliptical orbit, respectively. These two values correspond to an eccentricity $e^{\text{target}} = \frac{r_a^{\text{target}} - r_p^{\text{target}}}{r_a^{\text{target}} + r_p^{\text{target}}}$.

Once the capture has been obtained as in Section 4.2, the value of $r_a$ is close to $R^{\text{SOI}}$, which is much larger than $r_a^{\text{target}}$, while $r_p$ may already be of the order of $r_p^{\text{target}}$. Therefore, the main task of the transfer manoeuvre is to lower the apoapsis. Since according to Eq. (4) the rate of energy depletion is proportional to the velocity $v$, which is larger for smaller values of $r$, a convenient strategy to reach this goal is to turn on the deceleration around each pass through the periapsis.

Let $r_p^{\text{cap}} \ll R^{\text{SOI}}$ and $r_a^{\text{cap}} \sim R^{\text{SOI}}$ be the projected periapsis distance of the captured orbit obtained after the first pass. The additional specific energy required for lowering the trajectory to the target orbit can be obtained from Eq. (4), and reads,

$$\varepsilon|_{\text{lowering}} = \frac{\mu}{r_p^{\text{target}} + r_a^{\text{target}}} - \frac{\mu}{r_p^{\text{cap}} + r_a^{\text{cap}}} \simeq \frac{\mu}{2a^{\text{target}}} - \frac{\mu}{R^{\text{SOI}}}, \tag{10}$$

where $a^{\text{target}} = (r_p^{\text{cap}} + r_a^{\text{cap}})/2$ is the semimajor axis of the target orbit.

Since the manoeuvres cannot be made completely instantaneous, each pass around periapsis, besides lowering the apoapsis, also provokes a slight decrease in $r_p$. Therefore a special care should be payed to having $r_p^{\text{capture}}$ significantly larger than the target value $r_p^{\text{target}}$, otherwise the final periapsis could be lower than desired. In any case, the decelerating thrust should be applied in each turn close enough to the osculating periapsis $r_p$ for minimising the fuel requirements. In other words, it has to turned on when $r < r^{\text{low}}(r_p)$, where $r^{\text{low}}(r_p)$ is a convenient function of $r_p$. In the case considered for this study, choices around $r^{\text{low}}(p) = 1.2 r_p$ turn out to produce the most efficient transfer while keeping the total time of the manoeuvre within reasonable limits.

Fig. 12 shows a lowering manoeuvre reaching an orbit of periapsis height of 300 km above Mars surface and an apoapsis height of 1000 km. The thrusting arcs are also indicated (in red), corresponding in each turn to the points around the osculating periapsis distance $r_p$ within a 1.2 factor, as discussed above. This manoeuvre takes 800 days, and after the interplanetary transfer it is the most expensive manoeuvre in terms of mass consumption.

### 4.5. Combined analysis of the manoeuvres

In this section we present the combined analysis of the orbital manoeuvres, which have driven the design of the different subsystems as described in Section 3

Fig. 13 illustrates the mass consumption profile of the mission, spanning from the interplanetary phase up to the scientific phase where the nominal orbit is reached. The most substantial propellant utilisation occurs during the initial interplanetary transfer (384 kilograms), leading to a rendezvous with Mars with asymptotic relative velocity of 0.001 km/s. Such a nearly parabolic arrival in the SOI of the target planet allows for significantly reducing the propellant requirements for the subsequent capture manoeuvre, making it feasible with the chosen EP engine.

Once Mars' SOI is reached, the capture manoeuvre takes place. As depicted in Fig. 13, only a half of its duration involves mass consumption. The capture manoeuvre extends over 4.5 days and requires approximately 25 kilograms of propellant. Subsequently, the plane change manoeuvre is performed with a 10 days duration and a 12 kilograms of fuel consumption.

Finally, the circularisation phase takes place, representing the second most significant propellant consumption throughout the mission with 160 kilograms in 800 days. As the selection of the thrusting arc is also optimised, this mission phase has a considerable larger time length as compared with that of an impulsive $\Delta v$ manoeuvre using chemical propulsion. The mass consumption is also increased at the late stage of this phase due to the fact that the orbit is becoming more circular, so that the ignition condition $r < 1.2\,r_p$ is fulfilled for longer and longer arcs. This can also be understood by comparing the thrusting times of the circularisation phase, which can be extracted from the peaks of power consumption of Fig. 14, with the corresponding mass consumption.

Table 9 presents the duration and the mass consumption for each mission phase.

Fig. 14 shows the power generated by the solar array and the power consumed by the spacecraft through the mission, including the interplanetary transfer and the subsequent manoeuvres in the SOI of

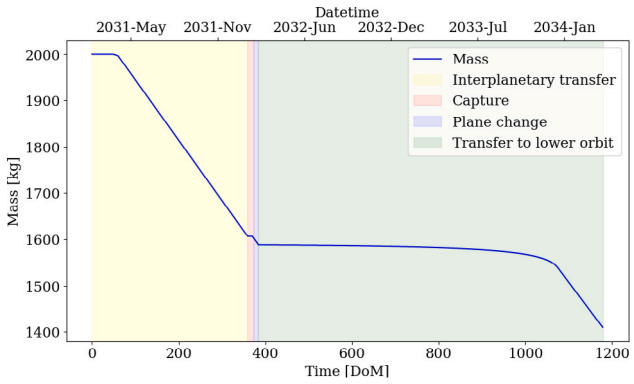


**Fig. 13.** Mass consumption until the beginning of the scientific phase expressing time in days of mission (DoM).

**Table 9**
Mass consumption and time duration of each trajectory phase. $M_i$ and $M_f$ correspond to the initial and final mass respectively, $\Delta m$ to the mass consumption and ToF is the time of flight of each phase.

| Mission phase | $M_i$ [kg] | $M_f$ [kg] | $\Delta m$ | ToF [days] |
|---|---|---|---|---|
| Interplanetary transfer | 2000 | 1616 | 384 | 363 |
| Insertion | 1616 | 1591 | 25 | 4.5 |
| Plane change | 1591 | 1579 | 12 | 10 |
| Circularisation | 1579 | 1419 | 160 | 800 |

Mars, up to completing the first year of the nominal phase. The distance to the sun, the eclipses with other solar system bodies and the decay of the power generation produced by the aging of the solar cells, have been taken into account for the power generation calculations.

The strong seasonal variation of the temporal behaviour in Fig. 14 is due to the polar inclination of the final orbit, which reduces the eclipse length and frequency in a substantial way. This fact allow us to reduce the battery and the solar array sizes in the lowering manoeuvre, in which the power consumption is large along the frequent thrusting arcs. During the nominal part of the mission, the power generated is considerably higher than the required one. This extra power can be profited by the payload, or allow for extending the mission duration.

Fig. 15 shows the capabilities of the battery to provide the required energy even during the thrusting arcs. The state of charge (SOC) of the battery is considerably reduced during the eclipses (≃13 min) when the EP is active. When EP is not active, the discharging rate is much slower (as visible in the second eclipse of the figure). The charging speed of the battery is also impacted by the thrusting arcs as it depends on the available power. We analysed the SOC of the battery through all the stages of the mission, and checked that they always provide the required energy, including during the eclipse seasons. Fig. 15 illustrates an example for a limited time span, and provides an insight on the discharge cycles of the battery.

## 5. Discussion

In this section we discuss the comparison between the proposed EP mission and an analog one using chemical propellant. The key variables to compare are the time and the mass consumption required to reach the final low orbit around Mars. To perform this analysis, we propagated backwards the $\Delta v$ required by a chemical mission to arrive in the final orbit by means of impulsive manoeuvres. With this approach, we obtained the initial mass at each mission phase. In particular, the launch mass is the minimum required mass to attain the same target polar orbit around Mars with the same final mass as in the EP concept discussed in Section 4. Here, the different manoeuvres will be described in chronological order.

**Table 10**
Main figures of an analog chemical mission considering a specific impulse of 300 s. $M_i$ and $M_f$ correspond to the initial and final mass respectively, $\Delta m$ to the mass consumption, $\phi$ to the ratio between the mass consumption in our EP proposal vs that using CP and ToF is the time of flight of each phase.

| Mission phase | $\Delta v$ [km/s] | $M_i$ [kg] | $M_f$ [kg] | $\Delta m$ | $\phi$ | ToF [days] |
|---|---|---|---|---|---|---|
| Interplanetary transfer | 2.37 | 4870 | 2175 | 2695 | 0.14 | 230 |
| Insertion | 0.015 | 2175 | 2164 | 11 | 2.27 | 3 |
| Plane change | 0.03 | 2164 | 2142 | 22 | 0.54 | 30 |
| Circularisation | 1.25 | 2142 | 1400 | 742 | 0.22 | 30 |

With these assumptions, we considered the same interplanetary scenario as in Section 4.1 and presented in Table 7, namely, a trajectory departing between 2030 and 2040 and a duration of 200 to 365 days.

The required $\Delta v$ at Mars arrival, depending on the chosen trajectory, are presented in Fig. 16. In the most optimal case, corresponding to a launch epoch of 2037-09-25 and of 230 days duration, the required $\Delta v$ to reduce the arrival velocity with respect to Mars up to 0.001 km/s, is of 2.37 km/s. Traditionally, fly-bys are used to reduce this value, however that would lead to longer time scales. Like for the EP mission considered in Section 4, we assumed that the first quasi-Hohmann $\Delta v$ at the departure is provided by the launcher. In this case, $C_3 = 34.62\ \mathrm{km}^2/\mathrm{s}^2$, which is still achievable with current launchers for the required launch mass ($\sim$ 5000 kg as discussed below).

Table 10 shows the $\Delta v's$ and masses needed to accomplish this mission concept with a chemical thruster having a typical specific impulse of 300 s [1]. In particular, the required propellant mass for the optimal Lambert transfer is 2695 kg, which is 7.1 times larger than that for the EP mission considered in Section 4.

As CP uses impulsive burns, the insertion in Mars' SOI can most conveniently be obtained by applying a $\Delta v$ in the opposite direction to the velocity around the periapsis, which can also be chosen to be close to the planet in order to profit from the Oberth effect [55]. The optimal choice is a periapsis height of 300 km, the value of the final target orbit. In this case, the insertion requires only 11 kg of propellant. This is the only phase of the mission for which the mass consumption using EP, which is 25 kg, is larger than that using CP. This is due to the fact that with EP the manoeuvre has to be performed along a thrusting arc whose points are at greater distances from the periapsis.

The optimal plane change manoeuvre for CP is obtained with a $\Delta v$ in the direction orthogonal to the orbital plane (+**W**) when the true anomaly reaches the value $\theta_m$ corresponding to the maximum value of $\dot{i}$, as in Section 4.3. The resulting mass consumption is 22 kg, which is larger than that of the EP mission by a factor of 2.

Finally, a single $\Delta v$ in the antiparallel direction to the velocity around the periapsis can be used to accomplish the circularisation phase with CP, and reach the target polar orbit between 300 and 1000 km of height. The mass consumption for this manoeuvre is 742 kg, which is larger by a factor of 5 than that for the EP mission.

Overall, a chemical mission would need a launch mass of 4870 kg to reach the target orbit, while our EP concept would require only 2000 kg. The main price to pay is a significantly longer duration of the circularisation manoeuvre (800 days with EP vs 30 days with CP). Therefore EP implies a 41% mass reduction, as compared with a similar CP Martian mission, still maintaining a reasonable time scale (3.2 years from launch, as compared with almost one year using CP) for reaching the circularised polar orbit around Mars. This result is in line with that of [20], according to which the required mass for a CP mission to Deimos and Phobos would require two times the mass of a similar SEP proposal.

## 6. Conclusions

We have shown that a mission to Mars using a solar electric propulsion (SEP) system is feasible with current technology. A comprehensive

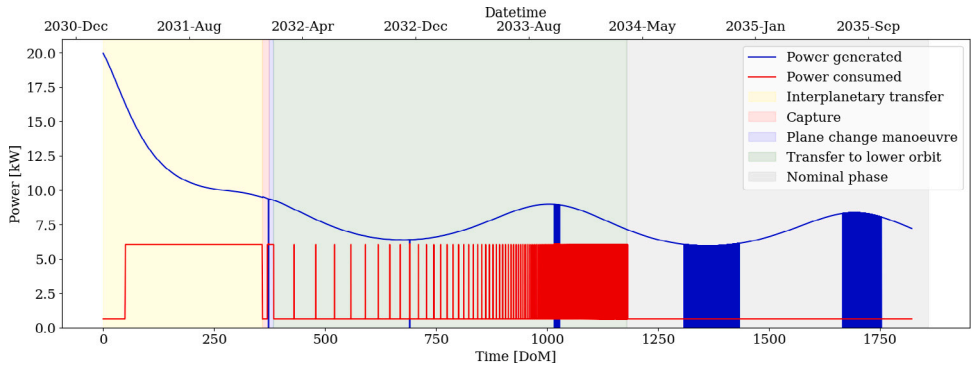


**Fig. 14.** Power consumption and generation through the mission up to the first year of the nominal phase.

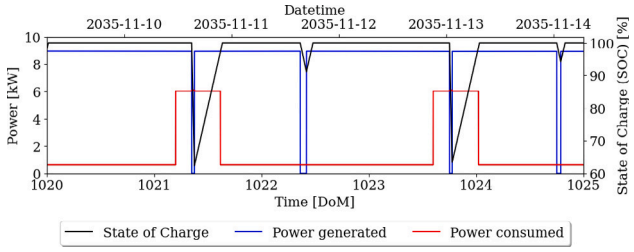


**Fig. 15.** Power consumption, generation and State of Charge of the battery on November 2035 (during transfer to lower orbit and eclipse season).

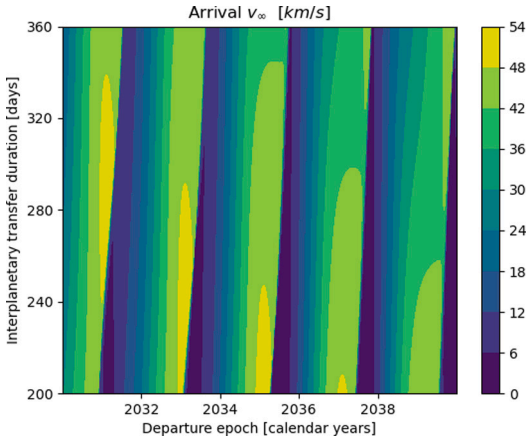


**Fig. 16.** Porkchop plot for an analog chemical mission in the scenario of our EP study.

analysis of the available state of the art on electric thrusters, also taking into account realistic mission requirements, allowed us to select the BHT-6000 engine. With this thruster, we designed a spacecraft of 2000 kg wet mass at launch, with reasonable mission constraints and operation concepts.

We presented a complete orbit analysis, including in-house optimisation methods for obtaining the interplanetary transfer to Mars within one year and with minimal fuel consumption. We also optimised the orbit insertion, the plane change manoeuvre attaining a polar Martian orbit, and the final circularisation around 300 and 1000 km of altitude. All these manoeuvres can be performed with the designed SEP system solely, as our power and mass analyses demonstrate, provided that the vehicle leaves the Earth orbit with a suitable specific energy that is attainable using current launchers. The required power is generated by a 30 $m^2$ solar array, supplemented by suitable batteries that ensure a continuous supply even during eclipse periods. This mission concept allows us to place a spacecraft with a dry mass of almost 1300 kg into a polar Martian orbit with 150 to 200 kg allocated for the scientific instruments.

The culmination of these orbital manoeuvres occurs over a two-year span, while the observation time of the mission could last for more than 5 years since it only requires minimal station-keeping adjustments.

We also presented a comparison of the propellant mass cost between our SEP concept and an analog chemically propelled mission. To achieve the same final mass at the target Martian polar orbit, a CP mission would need a launch mass of 4870 kg, which is larger by a factor of $\sim 2.4$ than the 2000 kg required for our SEP concept. This result highlights the key role that SEP can represent in future interplanetary missions.

Finally, we hope that the optimisation methods presented in this work may also be used as a baseline for the design of any future SEP mission to Mars.

## Declaration of competing interest

The authors declare that they have no known competing financial interests or personal relationships that could have appeared to influence the work reported in this paper.

## Acknowledgements

D.T. was funded by grants PID2020-118613GB-I00 (MCIN/AEI/10.13039/501100011033/) and ED431B 2021/22 (Xunta de Galicia, Spain). F.N-M. was funded by Spanish Ministry of Universities within the ”Jose Castillejo” program with reference number CAS21/00502. Funding for open access charge: Universidade de Vigo/CISUG.

## References

[1] Stéphane Mazouffre, Electric propulsion for satellites and spacecraft: established technologies and novel approaches, Plasma Sources. Sci. Technol. 25 (3) (2016) 033002.

[2] Dan Lev, Roger M. Myers, Kristina M. Lemmer, Jonathan Kolbeck, Hiroyuki Koizumi, Kurt Polzin, The technological and commercial expansion of electric propulsion, Acta Astronaut. 159 (2019) 213–227.

[3] Dan R. Lev, Gregory D. Emsellem, Ashley K. Hallock, The rise of the electric age for satellite propulsion, New Space 5 (1) (2017) 4–14.

[4] Les Johnson, Michael Meyer, Bryan Palaszewski, David Coote, Dan Goebel, Harold White, Development priorities for in-space propulsion technologies, Acta Astronaut. 82 (2) (2013) 148–152, 7th IAA Symposium on Realistic Advanced Scientific Space MissionsAosta, Italy, July 2011.

[5] Marc Rayman, Steven Williams, Design of the first interplanetary solar electric propulsion mission, J. Spacecr. Rockets 39 (2002) 589–595.

[6] Franklin Chang Díaz, John Carr, Les Johnson, William Johnson, Giancarlo Genta, P. Federica Maffione, Solar electric propulsion for human Mars missions, Acta Astronaut. 160 (2019) 183–194.

[7] Nargess Memarsadeghi, Lucy Mcfadden, David Skillman, Brian McLean, Max Mutchler, Uri Carsenty, Eric Palmer, The Group, Moon search algorithms for NASA’s dawn mission to asteroid vesta, Proc SPIE 8296 (2013).

[8] T.G. Müller, J. Durech, M. Ishiguro, M. Mueller, T. Krühler, H. Yang, M.-J. Kim, L. OŔourke, F. Usui, C. Kiss, B. Altieri, B. Carry, Y.-J. Choi, M. Delbo, J.P. Emery, J. Greiner, S. Hasegawa, J.L. Hora, F. Knust, D. Kuroda, D. Osip, A. Rau, A. Rivkin, P. Schady, J. Thomas-Osip, D. Trilling, S. Urakawa, E. Vilenius, P. Weissman, P. Zeidler, Hayabusa-2 mission target asteroid 162173 Ryugu (1999 JU3): Searching for the objectś spin-axis orientation, Astron. Astrophys. 599 (2017) A103.

[9] Ari Jonsson, Robert Morris, Liam Pedersen, Autonomy in space exploration: Current capabilities and future challenges, in: IEEE Aerospace Conference Proceedings, 2007, pp. 1–12.

[10] Christopher Rouff, Autonomy in future space missions, 2002.

[11] Joseph A. Starek, Behçet Açıkmeşe, Issa A. Nesnas, Marco Pavone, Spacecraft autonomy challenges for next-generation space missions, in: Eric Feron (Ed.), Advances in Control System Technology for Aerospace Applications, Springer Berlin Heidelberg, Berlin, Heidelberg, 2016, pp. 1–48.

[12] Richard Doyle, Spacecraft autonomy and the missions of exploration, Intell. Syst. Appl. IEEE 13 (1998) 36–44.

[13] Franklin Díaz, Mark Carter, Tim Glover, Andrew Ilin, Christopher Olsen, J. Squire, Ron Litchford, Nobuhiro Harada, Steven Koontz, Fast and robust human missions to Mars with advanced nuclear electric power and vasimr® propulsion, 2013.

[14] Daniel J. Dorney, A study for Mars manned exploration, Lunar Planet. Sci. Explor. 13 (2012).

[15] Andrew V. Ilin, Vasimr® human mission to Mars, in: Space, Propulsion & Energy Sciences International Forum, 2011.

[16] J. Dankanich, B. Vondra, A. Ilin, Fast transits to Mars using electric propulsion, in: 46th AIAA/ASME/SAE/ASEE Joint Propulsion Conference & Exhibit, 2012.

[17] John Dankanich, Bob Vondra, Andrew Ilin, Fast transits to Mars using electric propulsion, 2010.

[18] Douglas Fiehler, Steve Oleson, A comparison of electric propulsion systems for Mars exploration, in: 39th AIAA/ASME/SAE/ASEE Joint Propulsion Conference and Exhibit.

[19] Valerie Lyons, J. Gilland, D. Fiehler, Electric propulsion concepts enabled by high power systems for space exploration, in: 2nd International Energy Conversion Engineering Conference.

[20] Steven Oleson, Melissa McGuire, Tim Sarver-Verhey, Doug Fiehler, John Dankanich, Jeff Juergens, Tom Parkey, John Gyekenyesi, Jim Gilland, Tony Colozza, Tom Packard, Thahn Nguyen, Paul Schmitz, Phobos and deimos sample return mission using solar electric propulsion, in: AIAA SPACE 2009 Conference &Amp; Exposition.

[21] Marcus Langston, Matt Sorgenfrei, Ricardo Diaz-Silva, Federico Aguilar, Alvaro Fidalgo, A mission architecture for scientific exploration of a trojan object using solar electric propulsion, in: AIAA SPACE 2010 Conference &Amp; Exposition.

[22] Howard D. Curtis, Orbital Mechanics for Engineering Students, third ed., Butterworth-Heinemann, Boston, 2014.

[23] D. Pavarin, F. Ferri, M. Manente, D. Curreli, Y. Guclu, Melazzi Davide, D. Rondini, S. Suman, J. Carlsson, C. Bramanti, E. Ahedo, V. Lancellotti, K. Katsonis, G. Markelov, Design of 50 w helicon plasma thruster, in: Proceedings of the 31st International Electric Propulsion Conference, IEPC-2009, 20-24 September, 2009, Ann Arbor, Michigan, 2009, pp. 1–8.

[24] Benjamin Wachs, Benjamin Jorns, Optimization of an ECR thruster using two frequency and pulsed waveforms, in: AIAA Propulsion and Energy 2021 Forum.

[25] Miguel Sangregorio, Kan Xie, Ningfei Wang, Ning Guo, Zun Zhang, Ion engine grids: Function, main parameters, issues, configurations, geometries, materials and fabrication methods, Chin. J. Aeronaut. 31 (8) (2018) 1635–1649.

[26] Chengjin Huang, Jianling Li, Mu Li, Performance measurement and evaluation of an ionic liquid electrospray thruster, Chin. J. Aeronaut. 36 (3) (2023) 1–15.

[27] Kurt A. Polzin, Comprehensive review of planar pulsed inductive plasma thruster research and technology, J. Propuls. Power 27 (3) (2011) 513–531.

[28] Jinxing Zheng, et al., Integrated study on the comprehensive magnetic–feld confguration performance in the 150 kW superconducting magnetoplasmadynamic thruster, Sci. Rep. (2021).

[29] Jakob Balkenhohl, Jakub Glowacki, Nicholas Rattenbury, John Cater, A review of low-power applied-field magnetoplasmadynamic thruster research and the development of an improved performance model, J. Electr. Propuls. 2 (2023).

[30] Zhiwen Wu, Tiankun Huang, Xiangyang Liu, William Yeong Liang Ling, Ningfei Wang, Lucheng Ji, Application and development of the pulsed plasma thruster, Plasma Sci. Technol. 22 (9) (2020) 094014.

[31] Archit Bapat, Pramod B. Salunkhe, Aakash V. Patil, Hall-effect thrusters for deep-space missions: A review, IEEE Trans. Plasma Sci. 50 (2) (2022) 189–202.

[32] Pavlos G. Mikellides, Modeling and analysis of a megawatt-class magnetoplasmadynamic thruster, J. Propuls. Power 20 (2) (2004) 204–210.

[33] Maximilian Schadegg, Ryan Russell, Gregory Lantoine, Jovian orbit capture and eccentricity reduction using electrodynamic tether propulsion, 2014,

[34] R.D. Estes, E.C. Lorenzini, J. Sanmartin, J. Pelaez, M. Martinez-Sanchez, C.L. Johnson, I.E. Vas, Bare tethers for electrodynamic spacecraft propulsion, J. Spacecr. Rockets 37 (2) (2000) 205–211.

[35] Marco Casanova-Álvarez, Fermín Navarro-Medina, Daniele Tommasini, Conceptual design of electrodynamic multi tether system for self-propelled jovian capture, Acta Astronaut. 184 (2021) 299–307.

[36] M.C. Pereira, C.F. de Melo, L.G. Meireles, Numerical analysis of orbital transfers to Mars using solar sails and attitude control, J. Phys. Conf. Ser. 911 (1) (2017) 012026.

[37] Yufei Guo, Dongzhu Feng, Xin Wang, Cong Li, Yunzhao Liu, The Earth-Mars transfer trajectory optimization of solar sail based on hp -adaptive pseudospectral method, Discrete Dyn. Nat. Soc. 2018 (2018) 1–14.

[38] C. Mullins, V. Hruby, B. Pote, K. Blake, Development of a 5kW class hall thruster, in: 36th International Electric Propulsion Conference, University of Vienna, Vienna, Austria, 2019.

[39] European Space Agency, ExoMars factsheet, 2022.

[40] Eddy Neefs, Ann Carine Vandaele, Rachel Drummond, Ian R. Thomas, Sophie Berkenbosch, Roland Clairquin, Sofie Delanoye, Bojan Ristic, Jeroen Maes, Sabrina Bonnewijn, Gerry Pieck, Eddy Equeter, Cédric Depiesse, Frank Daerden, Emiel Van Ransbeeck, Dennis Nevejans, Julio Rodriguez-Gómez, José-Juan López-Moreno, Rosario Sanz, Rafael Morales, Gian Paolo Candini, M. Carmen Pastor-Morales, Beatriz Aparicio del Moral, José-Maria Jeronimo-Zafra, Juan Manuel Gómez-López, Gustavo Alonso-Rodrigo, Isabel Pérez-Grande, Javier Cubas, Alejandro M. Gomez-Sanjuan, Fermín Navarro-Medina, Tanguy Thibert, Manish R. Patel, Giancarlo Bellucci, Lieve De Vos, Stefan Lesschaeve, Nico Van Vooren, Wouter Moelans, Ludovic Aballea, Stijn Glorieux, Ann Baeke, Dave Kendall, Jurgen De Neef, Alexander Soenen, Pierre-Yves Puech, Jon Ward, Jean-François Jamoye, David Diez, Ana Vicario-Arroyo, Michel Jankowski, NOMAD spectrometer on the ExoMars trace gas orbiter mission: part 1 — design, manufacturing and testing of the infrared channels, Appl. Opt. 54 (2015) 8494–8520.

[41] Manish R. Patel, Philippe Antoine, Jonathon Mason, Mark Leese, Brijen Hathi, Adam H. Stevens, Daniel Dawson, Jason Gow, Timothy Ringrose, James Holmes, Stephen R. Lewis, Didier Beghuin, Philip van Donink, Renaud Ligot, Jean-Luc Dewandel, Daohua Hu, Doug Bates, Richard Cole, Rachel Drummond, Ian R. Thomas, Cédric Depiesse, Eddy Neefs, Eddy Equeter, Bojan Ristic, Sophie Berkenbosch, David Bolsée, Yannick Willame, Ann Carine Vandaele, Stefan Lesschaeve, Lieve De Vos, Nico Van Vooren, Tanguy Thibert, Emmanuel Mazy, Julio Rodriguez-Gomez, Rafael Morales, Gian Paolo Candini, M. Carmen Pastor-Morales, Rosario Sanz, Beatriz Aparicio del Moral, José-Maria Jeronimo-Zafra, Juan Manuel Gómez-López, Gustavo Alonso-Rodrigo, Isabel Pérez-Grande, Javier Cubas, Alejandro M. Gomez-Sanjuan, Fermín Navarro-Medina, Ali BenMoussa, Boris Giordanengo, Samuel Gissot, Giancarlo Bellucci, Jose Juan Lopez-Moreno, NOMAD spectrometer on the ExoMars trace gas orbiter mission: part 2 — design, manufacturing, and testing of the ultraviolet and visible channel, Appl. Opt. 56 (2017) 2771–2782.

[42] G. Peter, J. Helbert, H. Hiesinger, Iris Weber, Ingo Walter, Gabriele Arnold, Thomas Säuberlich, Developing of MERTIS as an advanced process from the study up to the flight model, 8867, 2013,

[43] Mission Studies Office, Science Future Mission Department, EPIG CDF study summary report, ESA 39 (2019) 1–54.

[44] S.A. Townes, F. Amoozegar, James Border, J.C. Breidenthal, D. Morabito, K.I. Moyd, J.E. Patterson, S. Shambayati, Operational demonstration of Ka-band telecommunications for the Mars reconnaissance orbiter, 2003, pp. 3565–3580.

[45] Jun Sun, Jay Gao, Shervin Shambayati, Eytan Modiano, Ka-band link optimization with rate adaptation for Mars and lunar communications, Int. J. Sat. Commun. Netw. 25 (2) (2007) 147–165.

[46] Shervin Shambayati, David Morabito, James Border, Faramaz Davarian, Dennis Lee, Ricardo Mendoza, Michael Britclie, Sander Weinreb, Mars reconnaissance orbiter Ka-band (32 GHz) demonstration: Cruise phase operations, 2006.

[47] A. Olea, A. Montesano, C. Montesano, S. Arenas, X- band high gain antenna qualified for Mars atmosphere, 2010.

[48] Frederick Krause, John-Paul Ruiz, Simon Jones, Erik Brandon, Eric Darcy, Christopher Iannello, Ratnakumar Bugga, Performance of commercial Li-ion cells for future NASA missions and aerospace applications, J. Electrochem. Soc. 168 (2021).

[49] NASA Official: Mike Carney, NASA launch services program (LSP) performance web site, 2022.

[50] Dario Izzo, PyGMO and PyKEP: Open source tools for massively parallel optimization in astrodynamics (the case of interplanetary trajectory optimization), 2012.

[51] Dario Izzo, Will Binns, dariomm098m, Alessio Mereta, Christopher Iliffe Sprague, dhennes, Bert Van den Abbeele, Chris Andre, Krzysztof Nowak, Nat Guy, Alberto Isaac Barquín Murguía, Pablo, Frédéric Chapoton, GiacomoAcciarini, Moritz v. Looz, dietmarwo, Mike Heddes, Anatoli Babenia, Baptiste Fournier, Johannes Simon, Jonathan Willitts, Mateusz Polnik, Sanjeev Narayanaswamy, The Gitter Badger, Jack Yarndley, esa/pykep: Optimize, Zenodo, 2020.

[52] Francesco Biscani, Dario Izzo, Wenzel Jakob, GiacomoAcciarini, Marcus Märtens, michiboo, Alessio Mereta, Cord Kaldemeyer, Sergey Lyskov, Sylvain Corlay, Moritz v. Looz, Benjamin Pritchard, Akash Patel, Manuel López-Ibáñez, Oliver Webb, tmiasko, Johan Mabille, Giacomo Acciarini, Kishan Manani, Axel Huebl, Alex Biddulph, jakirkham, hulucc, Jeongseok Lee, Andrea Mambrini, Doodle1106, Erik O'Leary, Felipe Lema, Huu Nguyen, Ivan Smirnov, esa/pagmo2: pagmo 2.17.0, Zenodo, 2021.

[53] James M. Buchanan, The relevance of Pareto optimality, J. Confl. Resolut. 6 (4) (1962) 341–354.

[54] Hussain Gulshan, Budak, Sadiq, Generalization of the bisection method and its applications in nonlinear equations, Adv. Continuous Discret Model. 18 (2023).

[55] Carl E. Mungan Philip Rodriguez Blanco, Rocket propulsion, classical relativity, and the oberth effect, Phys. Teach. 57 (2019) 439–441.